IEEE Access
Multidisciplinary | Rapid Review | Open Access Journal

Date of publication xxxx 00, 0000, date of current version xxxx 00, 0000.

Digital Object Identifier 10.1109/ACCESS.2017.Doi Number

Mid-infrared supercontinuum and frequency comb generations by different optical modes in a multimode chalcogenide strip waveguide

YUJUN CHENG[1], JINHUI YUAN[1,2], (Senior Member, IEEE), CHAO MEI[2], FENG LI[3], XIAN ZHOU[2], QIANG WU[4,5], BINBIN YAN[1], KUIRU WANG[1], CHONGXIU YU[1], KEPING LONG[2], (Senior Member, IEEE), AND P.K.A. WAI[3], (Fellow, IEEE)

[1] State Key Laboratory of Information Photonics and Optical Communications, Beijing University of Posts and Telecommunications, Beijing 100876, China

[2] Research Center for Convergence Networks and Ubiquitous Services, University of Science & Technology Beijing, Beijing 100083, China

[3] Photonics Research Centre, Department of Electronic and Information Engineering, The Hong Kong Polytechnic University, Hung Hom, Hong Kong

[4] Department of Physics and Electrical Engineering, Northumbria University, Newcastle upon Tyne, NE1 8ST, United Kingdom

[5] Key Laboratory of Nondestructive Test (Ministry of Education), Nanchang Hangkong University, Nanchang 330063, China

Corresponding authors: Jinhui Yuan (e-mail: yuanjinhui81@bupt.edu.cn), Feng Li (e-mail: enlf@polyu.edu.hk), and Qiang Wu (qiang.wu@northumbria.ac.uk)

This work was supported by the National Natural Science Foundation of China (61875238), Research Grant Council of the Hong Kong SAR China (PolyU152173/17E and PolyU152471/16E), and BUPT Excellent Ph.D. Students Foundation (CX2020319).

ABSTRACT Supercontinuum (SC) with broad bandwidth and high coherence is crucial in the SC-based frequency comb source generation. In this paper, we numerically investigate the mid-infrared (MIR) SC generations with the three optical modes (TE_{00}, TE_{10}, and TE_{20}) in a multimode chalcogenide (As_2Se_3) strip waveguide. The waveguide structure is carefully engineered to ensure that the pump pulses are propagated in the normal dispersion regions of the considered three optical modes. Highly coherent and octave-spanning MIR SCs are generated when the optimized pump pulse with 80-fs pulse duration, 3-kW peak power, and 3-μm center wavelength is used. Moreover, the nonlinear dynamics of the SC generation are numerically analyzed. Finally, the SC-based frequency combs are numerically demonstrated when a pulse train with a repetition rate of 50 MHz is used as the pump source and launched into the multimode As_2Se_3-based strip waveguide. It is believed that the generated MIR SC and SC-based frequency comb sources have important applications in biophotonics, metrology, and sensing.

INDEX TERMS Chalcogenide strip waveguide, different optical modes, supercontinuum, frequency comb

I. INTRODUCTION

Generation of optical frequency comb has attracted great research interests due to the broad applications in optical communication, metrology, molecular detection, etc [1], [2]. For example, the wavelength-division multiplexing as one of the key technologies in optical communication systems requires a large number of discrete-wavelength laser sources. They can be replaced by one frequency comb source produced through a single seed laser. Thus, the complexity and cost of the system are greatly reduced [3], [4]. In general, frequency comb sources can be obtained from mode-locked lasers, micro-resonator based Kerr comb, or supercontinuum (SC) generated in nonlinear fiber or waveguides [5]-[10]. However, direct generation of self-referenced frequency comb in mode locked lasers is currently impossible since no gain medium could cover the span of an octave. In contrast, octave spanning frequency combs are achievable by exciting Kerr comb in micro-resonators or SC in nonlinear optical medium. Kerr comb in micro-resonators is the most promising technique to fabricate on-chip comb sources [11]. However, there are still problems that impede the application of Kerr frequency comb sources. Due to the high quality factor (Q-factor), the intrinsic thermal effect will cause instability of the source.

This article has been accepted for publication in a future issue of this journal, but has not been fully edited. Content may change prior to final publication. Citation information: DOI 10.1109/ACCESS.2020.3036282, IEEE Access

Another problem that limits the application is the challenging fabrication of the high Q-factor micro-resonators [12]. Compared with Kerr comb sources, the generation of SC-based frequency comb is much easier to launch a pump pulse train into a nonlinear fiber or waveguide. Before the thermal and fabrication problems of Kerr comb sources are solved, it is expected that SC-based frequency comb generation will serve as the preferred technique to be adopted in applications.

The dynamics that contribute to the SC generation including modulation instability (MI), soliton fission, four wave mixing (FWM), dispersive wave generation, and Raman scattering have been systematically investigated [13]. The group velocity dispersion at the pump launching wavelength and higher-order dispersion coefficients over the whole spectral range are critical effects that determine the quality of the SC generated [13], [14]. The SC generation pumped at anomalous dispersion region has been studied a lot owing to the large bandwidth benefiting from the combined contribution of all effects mentioned above. However, the perturbation sensitivity of MI greatly degrades the coherence of SC generated with pump pulses accompanied by noise [15]. A method of generating the coherent SC is to design nonlinear media with all-normal dispersion (ANDi) profile within the wavelength of interest [16], [17]. The incoherent processes of MI will be well suppressed. Recently, Milan et al. experimentally reported the coherent SC generation through a simple post-process technique to control the waveguide dispersion to obtain ANDi profile in a hybrid chalcogenide/silicon-germanium system [18]. Yuan et al. experimentally demonstrated a coherent SC by using ANDi chalcogenide all-solid microstructured fiber [19]. Fang et al. numerically achieved a three-octave coherent SC using ANDi Si_3N_4 slot waveguide [20]. When the pump pulses are launched and propagate into a normal dispersion waveguide, the spectral broadening is mainly induced by the self-phase modulation (SPM) and optical wave breaking (OWB) [21]. The SPM and OWB effects are self-seeded processes, which are coherent processes, degradation of the coherence of the generated SC will be avoided [22], [23]. However, there are still some limitations for coherent SC generation in ANDi region when the pump pulse duration or the propagation length is increasing [24], [25]. The reasonable pulse duration and propagation length need to be carefully selected. Besides the dispersion effect, the nonlinearity of waveguide is also important for SC generation. Adoption of materials with high Kerr nonlinearity and low nonlinear loss can enhance the nonlinear processes, which are beneficial to the SC generation.

Chalcogenide glasses are considered as one of the promising materials for mid-infrared (MIR) SC generations [26]-[29]. For example, the transparency window of As_2Se_3 is in the wavelength range from 0.85 to 17.5 μm [28]. However, the research works are mainly focusing on the MIR SC generation by the fundamental mode of chalcogenide waveguide [29]-[32]. Obviously if the pump light is coupled into a higher-order mode of the waveguide, the nonlinear dynamics of the MIR SC generation will be different to that with fundamental mode because of the remarkable difference in the dispersion characteristics [33], [34]. In this paper, we will investigate the MIR SC generations by different optical modes, which have potential applications in mode-division multiplexing and multimode sensing systems. Highly coherent and octave-spanning MIR SCs are generated in a multimode chalcogenide (As_2Se_3) strip waveguide by using three optical modes (TE_{00}, TE_{10}, and TE_{20}), which are designed with ANDi profiles within the wavelength of interest. SC-based frequency combs are achieved when a pulse train with 50 MHz repetition rate is used as the pump source. The paper is organized as follows: In Section II, we design a multimode As_2Se_3-based strip waveguide, and introduce the theoretical model. In Section III, the MIR SC generations with the three optical modes are numerically investigated with variation of pump parameters. Generation of octave-spanning MIR frequency combs are demonstrated with the pulse train. Conclusions are drawn in Section IV.

II. WAVEGUIDE DESIGN AND THEORETICAL MODEL

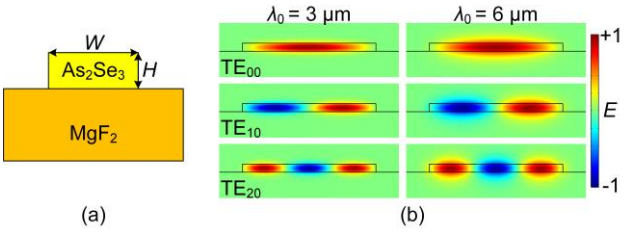

FIGURE 1. (a) The cross-section of the designed waveguide. (b) The normalized mode field distributions of the three quasi-TE modes (TE_{00}, TE_{10}, and TE_{20}) calculated at wavelengths 3 and 6 μm. The sign change in the scale bar indicates a shift in the phase of the electric field.

Fig. 1(a) shows the cross-section of the designed As_2Se_3 strip waveguide on a MgF_2 substrate. The As_2Se_3 waveguide has a width W of 14 μm and a height H of 0.8 μm. The thickness of the MgF_2 substrate used is 5.0 μm in the simulation. The fabrication of such a waveguide has been developed [35], [36]. It can be fabricated through the film deposition with thermal evaporation [37], photolithography [38], inductively coupled plasma etching with the CF_4/O_2 gas mixture or CHF_3 gas [39], [40], and photoresist removing by wet chemical stripping [41]. The refractive indices of As_2Se_3 and MgF_2 are calculated by the Sellmeier equation

$$n^2(\lambda) = 1 + \sum_{j=1}^{m} \frac{B_j \lambda^2}{\lambda^2 - \lambda_j^2}, \quad (1)$$

where λ is the wavelength. The coefficients of the Sellmeier equation for As_2Se_3 and MgF_2 are given in Table 1.

This article has been accepted for publication in a future issue of this journal, but has not been fully edited. Content may change prior to final publication. Citation information: DOI 10.1109/ACCESS.2020.3036282, IEEE Access

TABLE 1. Sellmeier coefficients for As_2Se_3 and MgF_2.

Material	As_2Se_3 [42]		MgF_2 [30]	
m	3		3	
	B_j	λ_j (μm)	B_j	λ_j (μm)
$j=1$	4.994872	0.24164	0.48755708	0.043384
$j=2$	1.712369	0.48328	0.39875031	0.09461442
$j=3$	0.120715	19.0	2.3120353	23.793604

With the full-vector finite element method (FEM), the mode field distributions of the three quasi-TE modes (TE_{00}, TE_{10}, and TE_{20}) calculated at wavelengths 3 and 6 μm are shown in Fig. 1(b). From Fig. 1(b), most of the mode field energy is well confined in the waveguide.

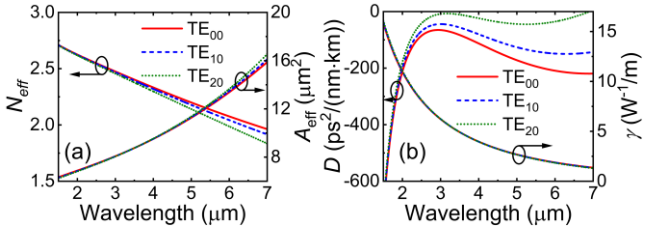

FIGURE 2. (a) The effective refractive index N_{eff} and effective mode area A_{eff} for the three optical modes TE_{00}, TE_{10}, and TE_{20}, and (b) group-velocity dispersion D and Kerr nonlinear coefficient γ for the TE_{00}, TE_{10}, and TE_{20} modes, respectively.

The effective refractive index N_{eff} and effective mode field area A_{eff} at different wavelengths for the three optical modes are shown in Fig. 2(a), which are also calculated by the full-vector FEM. From Fig. 2(a), the differences of N_{eff} and A_{eff} for different modes are enlarged as the wavelength increases. The group-velocity dispersion D is derived from N_{eff} as [43]

$$D(\lambda) = -\frac{\lambda}{c}\frac{d^2 N_{eff}}{d\lambda^2}, \tag{2}$$

where c is the velocity of light in vacuum. Fig. 2(b) shows the $D(\lambda)$ curves for the three optical modes. From Fig. 2(b), all three optical modes show all-normal dispersion within the wavelength range considered. Among them, the dispersion profile of TE_{20} mode is closest to the zero dispersion and flattest, which will be benefit to the SC generation. The dispersion profile of TE_{20} mode is the critical consideration in engineering the ANDi. When only H increases, all the dispersion curves go up in the same trend. As H increases to ~0.85 μm, the dispersion curve of TE_{20} mode begins to enter the anomalous region while the other two modes are still in the normal region. When only W decreases, all the dispersion curves go up at different levels. The TE_{20} mode is much sensitive to the change of W. As W decreases to ~13.5 μm, the dispersion curve of TE_{20} mode also begins enter the anomalous region while the other two modes are still in the normal region. To keep all three optical modes in the ANDi region, W of 14 μm and H of 0.8 μm are selected as optimized values. And the robustness in W and H are within 500 and 50 nm, respectively. The Kerr nonlinear coefficients γ can be calculated from n_2 and A_{eff}, which is related to the integration on the whole waveguide cross-section [43]

$$\gamma(\lambda) = \frac{2\pi n_2}{\lambda A_{eff}} = \frac{2\pi}{\lambda}\frac{\iint n_2(x,y)|F(x,y)|^4 dxdy}{\left(\iint |F(x,y)|^2 dxdy\right)^2}, \tag{3}$$

where $F(x,y)$ is the distribution of the mode fields and $n_2=2.4\times10^{-17}$ m²/W is the nonlinear refractive index of As_2Se_3 [42]. The $\gamma(\lambda)$ curves of the three optical modes are shown in Fig. 2(b). From Fig. 2(b), the three curves are mostly overlapped, which means they have almost same nonlinearity. This is mainly because the small deviation of A_{eff} between the three optical modes. The evolution dynamics of the short pulse propagating in the designed waveguide are modelled by a generalized nonlinear Schrödinger equation [31], [32]

$$\frac{\partial A}{\partial z} + \frac{\alpha}{2}A - \sum_{m\geq 2} i^{m+1}\frac{\beta_m}{m!}\frac{\partial^m A}{\partial t^m} = i\gamma\left(1+\frac{i}{\omega_0}\frac{\partial}{\partial t}\right)\left[A\int_0^\infty R(T)|A(z,t-T)|^2 dT\right], \tag{4}$$

where A is the slowly varying envelope in a retarded frame T, β_m (m=2, 3, …, and 13) is the mth-order dispersion coefficient calculated from a Taylor expansion of the propagation constant at the carrier frequency of the pump pulse, and α is the linear loss coefficient. R is the nonlinear response function as following

$$R(t) = (1-f_R)\delta(t) + f_R h_R(t), \tag{5}$$

where f_R, $\delta(t)$, and $h_R(t)$ are the fractional contribution of the Raman response, instantaneous electronic response, and delayed Raman response function, respectively. $h_R(t)$ is described by the Green's function of a damped harmonic oscillator, which is expressed as

$$h_R(t) = \frac{\tau_1^2+\tau_2^2}{\tau_1\tau_2^2}\exp\left(-\frac{t}{\tau_2}\right)\sin\left(\frac{t}{\tau_1}\right), \tag{6}$$

where τ_1 is the Raman period corresponding to the phonon oscillation frequency and τ_2 is the Raman gain spectral bandwidth. Some parameters used in the simulations are listed in Table 2 [40], [44], [45].

TABLE 2. Some parameters used in the simulations

Parameters	Waveguide length	α	f_R	τ_1	τ_2
Unit	cm	dB/cm	Null	fs	fs
Value	1	3	0.115	23.1	195

The coherence of SC is a key indicator to evaluate the quality of the SC generated. To quantify the coherence of SC, three important factors are calculated as following [46], [47]

$$\left|g_{1,2}^{(1)}(\lambda)\right| = \left|\frac{\left\langle A_1^*(\lambda)A_2(\lambda)\right\rangle}{\sqrt{\left\langle|A_1(\lambda)|^2\right\rangle\left\langle|A_2(\lambda)|^2\right\rangle}}\right|, \tag{7}$$

This article has been accepted for publication in a future issue of this journal, but has not been fully edited. Content may change prior to final publication. Citation information: DOI 10.1109/ACCESS.2020.3036282, IEEE Access

$$R = \frac{\int_0^\infty \left| g_{12}^{(1)}(\lambda) \right| \cdot P(\lambda) d\lambda}{\int_0^\infty P(\lambda) d\lambda}, \tag{8}$$

$$K = \lg(1 - R). \tag{9}$$

where $g_{1,2}^{(1)}$ is the first-order degree of coherence, which indicates the correlation of the signals from shot-to-shot at wavelength λ. $A_k(\lambda)$ is the spectral amplitude of the SC generated with the k-th shot pump pulse with random noise. The angular brackets denote the ensemble average among the independent pairs of the generated spectra. The weighted degree of coherence R in (8) measures the averaged coherence in the whole spectrum, where $P(\lambda)=\langle|A(\lambda)|^2\rangle$ denotes the ensemble average power spectrum of the generated SC. In (9), K is used to enlarge the detail of R when it is close to 1 for highly coherent SC.

III. SIMULATION RESULTS AND DISCUSSION

As the base of frequency comb, generation of SC with large bandwidth and high coherence is first investigated. By using the Runge-Kutta method with adaptive step-size to solve (4), the evolution dynamics of the SC generation can be characterized [48]. In the following simulation, the number of the frequency bins is chosen as 2^{15}. And the up to 13th-order dispersion coefficients are considered. A hyperbolic secant pulse with a complex amplitude of $P_0^{1/2}\mathrm{sech}(t/T_0)$ are used as the pump and coupled into the three optical modes TE_{00}, TE_{10}, and TE_{20} of the designed waveguide with a length of 1 cm, respectively. The coupling efficiency can be improved through designing the tapered couplers at both ends of the waveguide [49]. And the other two higher-order modes can be efficiently excited by the TE_{00} mode based on the tapered directional coupler scheme [50], [51]. In this section, we will vary the launching wavelength, peak power and pulse duration respectively to investigate the impact of these parameters and seek for appropriate parameter combination that should be used to optimize the performance of the SC generated.

We first investigate the impact of launching wavelength of the pump pulse. The pulse duration T_0 = 240 fs and peak power P_0 = 2 kW, which are moderate values to model the typical trends of dynamics along the variation of λ_0=2.5, 3, and 3.5 μm. Such laser sources centered at the three wavelengths are available from the previous works [52]-[54]. By using the dispersion and nonlinearity parameters of TE_{00}, TE_{10}, and TE_{20} modes, respectively, the spectral and temporal profiles of the SCs generated at the output point of the waveguide are shown in Fig. 3. In Figs. 3(a) and 3(b), when a pump pulse at λ_0=2.5 μm is coupled into the TE_{00} mode, the −40 dB bandwidth of the generated SC spans from 1.6 to 4.0 μm, covering 1.26 octaves. As λ_0 is increased to 3 and 3.5 μm, the SC is also shifted towards longer wavelength with simultaneous increase of the bandwidth. The −40 dB bandwidths of the generated SCs with 3 and 3.5 μm pump pulses span from 1.7 to 4.5 μm and 2.0 to 5.0 μm, respectively, covering 1.49 and 1.59 octaves. Besides, the spectral and temporal shapes of the generated SCs are asymmetric, and some burrs appear in the temporal profile due to the asymmetric dispersion profile. For the SC generation, because the pump pulses are launched at wavelengths with normal dispersions, SPM is the dominating nonlinear process at the initial stage. Then, the OWB, which is caused by the third-order dispersion and self-steepening, further broadens the optical spectra.

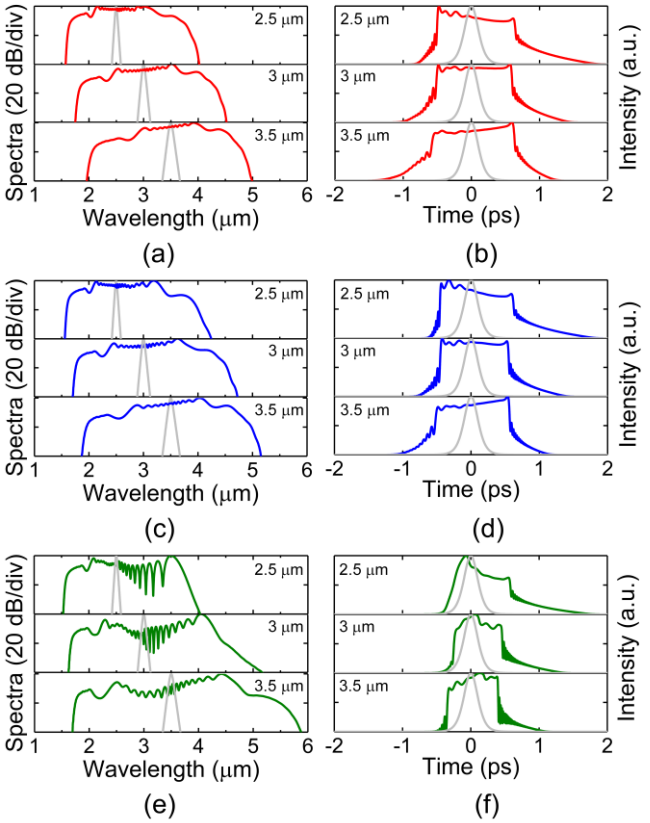

FIGURE 3. The spectral (left column) and temporal (right column) profiles of the SC generated when pump pulses with width T_0 of 240 fs and peak power P_0 of 2 kW are operated at wavelengths 2.5, 3, and 3.5 μm and coupled into the three optical modes TE_{00} ((a) and (b)), TE_{10} ((c) and (d)), and TE_{20} ((e) and (f)), respectively. The input pulses are also shown with the grey lines.

Figs. 3(c) and 3(d) show the spectral and temporal profiles of the SCs generated with TE_{01} mode and pump condition same to that of Figs. 3(a) and 3(b). The spectral and temporal profiles are similar to those shown in Figs. 3(a) and 3(b). For the TE_{10} mode, the −40 dB bandwidths of the SCs cover 1.43, 1.6, and 1.72 octaves, respectively. When the pump pulse is coupled into the TE_{20} mode, the spectral and temporal profiles of the generated SCs show notable differences as shown in Figs. 3(e) and 3(f). The SCs cover 1.33, 1.83, and 2.07 octaves with pump pulses at 2.5, 3, and 3.5 μm, respectively. The oscillation structures on the spectra mainly caused by enhanced SPM effect compared to TE_{00} and TE_{10} modes. Its dispersion is reduced since the dispersion curve of the TE_{20} mode is much closer to zero than TE_{00} and TE_{10} modes in most spectral region considered, which is beneficial to the nonlinear spectral

This article has been accepted for publication in a future issue of this journal, but has not been fully edited. Content may change prior to final publication. Citation information: DOI 10.1109/ACCESS.2020.3036282, IEEE Access

broadening. In addition, it is worth noting that when λ_0 is further shifted from 3 to 3.5 μm, the bandwidth increments of the SCs are not obvious except for the TE_{20} mode. The long wavelength part of the SC generation of TE_{20} mode is enhanced, but the pump sources with center wavelength above 3 μm are difficult to obtain. Therefore, λ_0 is chosen as 3 μm in the following discussion.

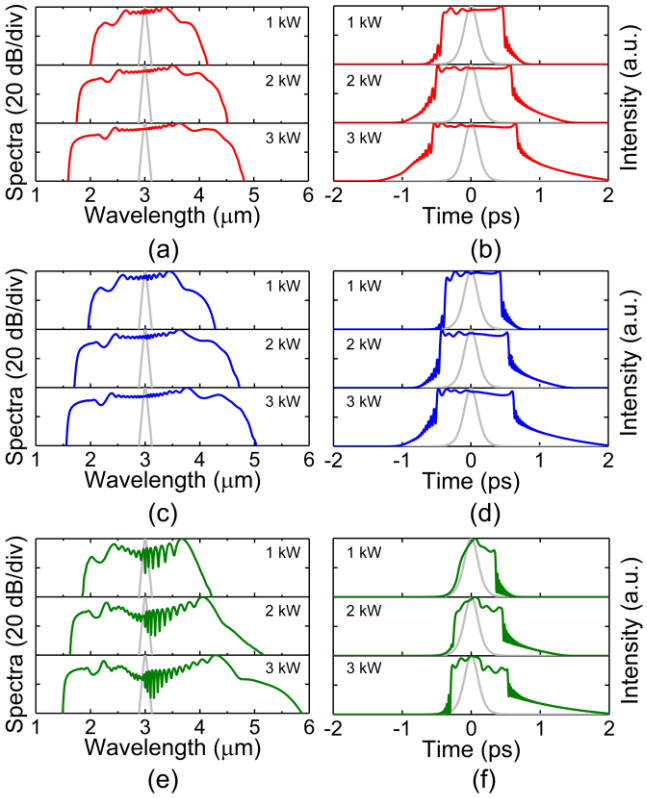

FIGURE 4. The spectral (left column) and temporal (right column) profiles of the SC generated when the pump pulses with λ_0= 3 μm and T_0=240 fs are coupled into the three optical modes TE_{00} ((a) and (b)), TE_{10} ((c) and (d)), and TE_{20} ((e) and (f)) for P_0=1, 2, and 3 kW, respectively. The input pulses are also shown with the grey lines.

Except for the launching wavelength λ_0, the peak power P_0 also plays an important role in the SC generation. In Fig. 4, we show the comparison of the generated SC with λ_0=3 μm and T_0=240 fs while the peak power is varied as P_0=1, 2, and 3 kW. The three rows of Fig. 4 show the results with TE_{00}, TE_{10}, and TE_{20} modes, respectively. When the pump pulse is launched into TE_{00} mode as shown in Figs. 4(a) and 4(b), the optical spectra extend on both sides due to the SPM effect and reach 1.10, 1.47, and 1.69 octaves for P_0=1, 2, and 3 kW, respectively. Figs. 4(c) and 4(d) show the results obtained with the TE_{10} mode. The –40 dB bandwidths of the generated SCs cover 1.21, 1.59, and 1.79 octaves, respectively, which are slightly larger than those of the TE_{00} mode. The –40 dB bandwidths of the SCs are further extended to 1.24, 1.83, and 2.13 octaves with the TE_{20} mode. Compared with the results shown in Figs. 4(a) to 4(d), the spectral and temporal profiles of the SCs with TE_{20} mode are asymmetric and show some oscillating structures. According to the results shown in Figs. 4(a) to 4(f), the optimized P_0=3 kW is used in the following discussions.

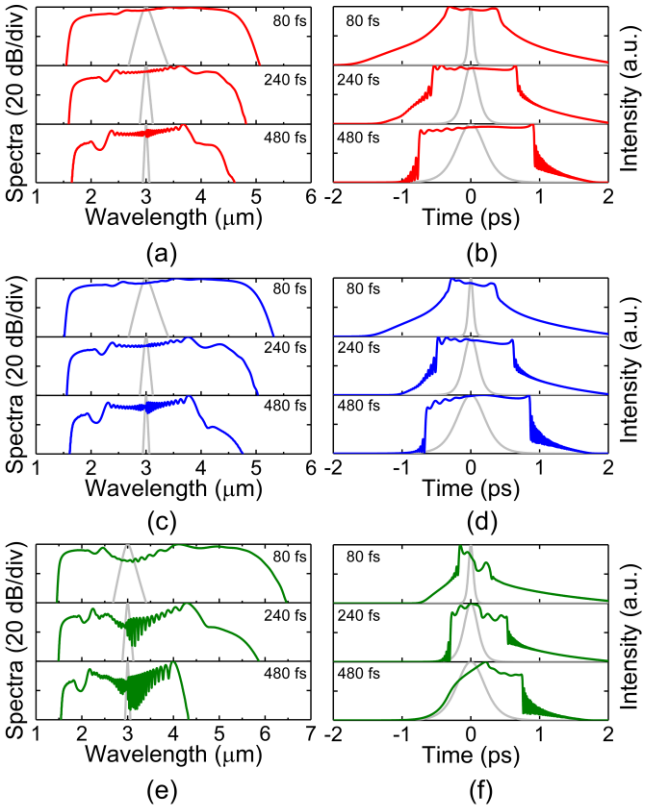

FIGURE 5. The spectral (left column) and temporal (right column) profiles of the SC generated when the pump pulses with λ_0=3 μm and P_0 =3 kW are coupled into the three optical modes TE_{00} ((a) and (b)), TE_{10} ((c) and (d)), and TE_{20} ((e) and (f)) for T_0 =80, 240, and 480 fs, respectively. The input pulses are also shown with the grey lines.

The influence of T_0 on the SC generation is also investigated. Figs. 5(a) to 5(f) show the spectral and temporal profiles of the SCs when pump pulses with λ_0=3 μm and P_0 =3 kW are operated at T_0 =80, 240, and 480 fs and coupled into the TE_{00}, TE_{10}, and TE_{20} modes, respectively. In Figs. 5(a) and 5(b), when the pump pulses with T_0=80, 240, and 480 fs are coupled into the TE_{00} mode, the –40 dB bandwidths of the SCs cover 1.82, 1.69, and 1.57 octaves, respectively. When the TE_{10} mode is chosen, the –40 dB bandwidths of the SCs are slightly increased to 1.93, 1.79, and 1.66 octaves, respectively, as shown in Figs. 5(c) and 5(d). The performance of the SCs with the TE_{20} mode are some different, the –40 dB bandwidths of the SCs cover 2.33, 2.13, and 1.48 octaves, respectively. The bandwidths of SCs pumped with 80 and 240 fs pulses are significantly enhanced comparing with the other two modes. However, the SC bandwidth pumped with 480 fs pulse is decreased. Comparing the results shown in Fig. 5, it is obvious that the SCs with the 80-fs pump pulse have the best performance in optimizing the bandwidth and flatness. The main reason can be explained as following. The pulse energy will be increased when P_0 is fixed and T_0 increases. At the same time, its initial bandwidth gradually becomes narrower. Each

This article has been accepted for publication in a future issue of this journal, but has not been fully edited. Content may change prior to final publication. Citation information: DOI 10.1109/ACCESS.2020.3036282, IEEE Access

wavelength part will have more energy. The nonlinear effect will be enhanced. Many oscillations appear when the pulse with duration of 480 fs is used. The flatness of SC becomes poor. Besides, the narrow initial bandwidth limits the spectral broadening because the number of frequency components participated in the initial SPM and OWB stages might be less than the shorter duration pulse which has larger initial bandwidth. Therefore, compared with the 240-fs and 480-fs pump pulses, the 80-fs pump pulse has the best performance for generating the flat and broadband SC.

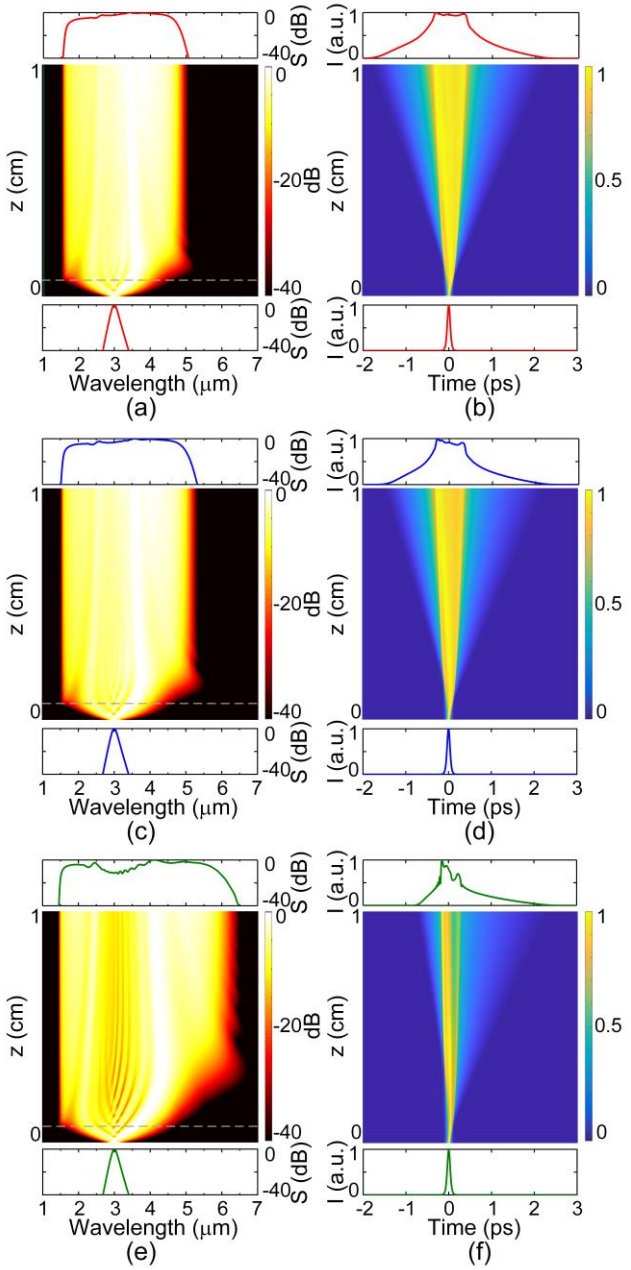

FIGURE 6. **The evolutions of the spectral (left column) and temporal (right column) profiles of the pump pulses along z for the three optical modes TE_{00} ((a) and (b)), TE_{10} ((c) and (d)), and TE_{20} ((e) and (f)), respectively, when pump pulses with λ_0 =3 μm, P_0 =3 kW, and T_0 =80 fs are used. The instantaneous spectral and temporal profiles at the input and output of the waveguide are also shown at the bottom and top of the evolution diagrams. The grey dash lines indicate z = 0.05 cm.**

Based on the above investigation, the optimized parameter combination λ_0=3 μm, P_0=3 kW, and T_0=80 fs will be used to study the evolutions of the SC signal. Fig. 6 shows the evolutions of the spectral and temporal profiles along the propagation of the pump pulse for the TE_{00}, TE_{10}, and TE_{20} modes. In Figs. 6(a) and 6(b), the pump pulses with λ_0=3 μm, P_0=3 kW, and T_0=80 fs are coupled into the TE_{00} mode. At the initial stage, the SPM plays an important role. The optical spectrum of the pump pulse broadens symmetrically and shows some oscillations. After the propagation of ~0.05 cm, the OWB effect becomes obvious, and sidelobes emerge on both sides of the optical spectrum. New frequency components are generated at the leading and trailing edges of the pump pulses through the four-wave mixing effect. The sidelobe on the short wavelength side emerges earlier. It is mainly due to the self-steepening effect [23]. With further propagation, the broadening of spectrum on blue side is terminated because of the large dispersion in the spectral region of <2 μm. The shape of the generated SC becomes asymmetric gradually because of the continuous broadening on red side. In the time domain, the pulse duration is broadened monotonously with the increase of the propagation length. The evolutions of SC in the TE_{10} mode are similar with those of the TE_{00} mode. However, the evolutions with the TE_{20} mode shown in Figs. 6(e) and 6(f) are significantly different to those with the TE_{00} and TE_{10} modes. Deep oscillations appear on the spectrum during the spectral broadening at very early stage, and gradually disappear after the propagation in a long distance. The oscillations decrease a lot near z = 1 cm. The SC in the TE_{20} mode extends on the long wavelength side to much longer wavelength than those of the TE_{00} and TE_{10} modes. And the increment in bandwidth does not change obviously near z = 1 cm. That is why we chose 1 cm as the length of waveguide. Finally, the SCs generated with the TE_{00}, TE_{10}, and TE_{20} modes reach 1.82, 1.93, and 2.33 octaves, respectively.

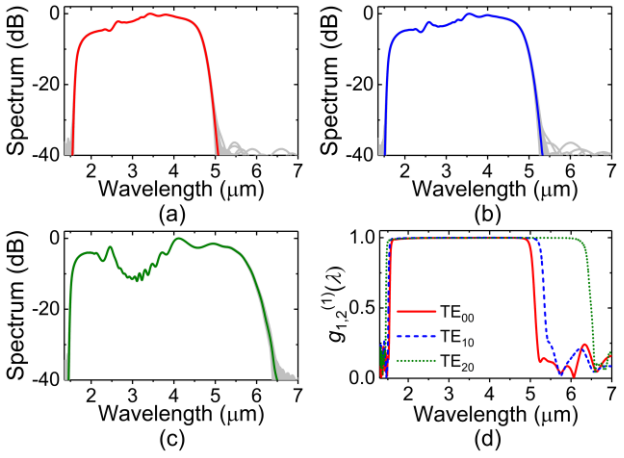

FIGURE 7. **The generated SCs with a noise level η = 0.01 for the three optical modes (a) TE_{00}, (b) TE_{10}, and (c) TE_{20}. The grey lines are the overlapped spectra of the 50 shots. The red, blue, and olive lines represent the averaged spectra of the 50 shots, respectively. (d) The first-order degree of coherence $g_{1,2}^{(1)}$ of the generated SCs with the TE_{00}, TE_{10}, and TE_{20}modes when η = 0.01.**

This article has been accepted for publication in a future issue of this journal, but has not been fully edited. Content may change prior to final publication. Citation information: DOI 10.1109/ACCESS.2020.3036282, IEEE Access

Besides the spectral bandwidth, the coherence of SCs is an important feature that determines the quality of frequency comb that based on the SC generation. To investigate the coherence of the generated SCs, the first-order degree of coherence $g_{1,2}^{(1)}$ is used. Figs. 7(a) to 7(d) show the generated SCs and $g_{1,2}^{(1)}$ calculated with 50 shot pump pulses with the one-photon-per-mode quantum noise [13], [46]. The random noise is individually generated for each shot by $n=\eta N\exp(i2\pi U)$, where η is the noise factor denoting the amplitude of the noise relative to the input pulse amplitude, N is a random variable with the standard normal distribution, and U is a random variable with the uniform distribution between 0 to 1 [46]. A noise level of η=0.01 is used in the simulation. In Figs. 7(a) to 7(c), the grey plots are the overlapped SC spectra of the 50 shots for the TE_{00}, TE_{10}, and TE_{20} modes, respectively. The red, blue, and olive curves in Figs. 7(a)-7(c) represent the averaged spectra of each 50 shots. All the generated spectra show slight variations from shot to shot. The calculated $g_{1,2}^{(1)}$ of the three modes are shown in Fig. 7(d). From Fig. 7(d), $g_{1,2}^{(1)}$ is almost 1 in the whole wavelength ranges considered, which indicates a high coherence of the SCs.

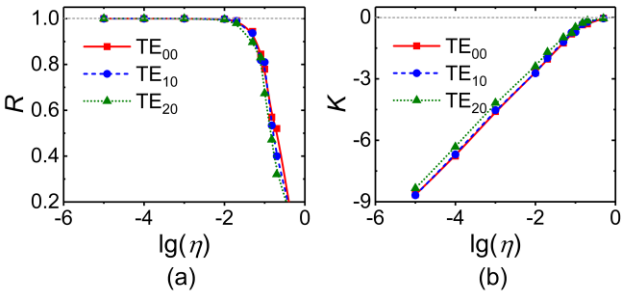

FIGURE 8. The weighted degree of coherence (a) *R* and (b) *K* as functions of lg(*η*) for the three optical modes TE_{00}, TE_{10}, and TE_{20}, respectively.

To quantify the coherence and the stability of the SCs, we simulated the SC generation with different noise levels and calculate the weighted degree of coherence R. Fig. 8(a) shows the relationship between R and lg(η) in the whole spectral range for the three modes considered. The values of R for the TE_{00}, TE_{10}, and TE_{20} mode are 0.52, 0.40, and 0.32 at lg(η=0.2). It implies that the TE_{00} mode may have slightly better noise tolerance than the TE_{10} and TE_{20} modes when η is high. For all the three modes, the value of R increases as lg(η) decreases, and it is very close to 1 when lg(η)$\leqslant$−2. The variable K is also plotted in Fig. 8(b) since R is close to 1 when lg(η)$\leqslant$−2. It can be seen from Fig. 8(b) that the three curves are very close, and the difference between the values of K for the modes are not obvious when lg(η) $\leqslant$ −2. Thus, the SCs generated by the considered three modes are highly coherent when $\eta\leqslant$0.01.

In order to demonstrate the generation of octave-spanning SC-based frequency comb, we launch a train of 50 pulses with 50 MHz repetition rate into the designed waveguide. The frequency combs generated by the TE_{00}, TE_{10}, and TE_{20} modes are shown in Figs. 9(a), 9(b), and 9(c), respectively. The shaded color regions represent the highly dense frequency combs. The zoom-in views shown as the insets clearly illustrate the fine frequency comb lines with an interval of 50 MHz which equals to the repetition rate of the seed pulse train.

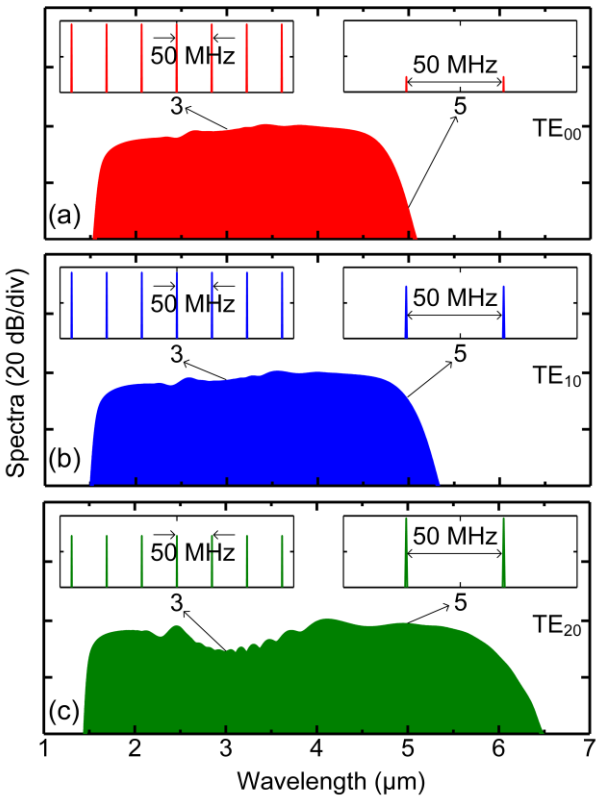

FIGURE 9. Frequency combs generated by 50 pulses with 50 MHz repetition rate for the three optical modes (a) TE_{00} (red), (b) TE_{10} (blue), and (c) TE_{20} (olive), respectively. The shaded color areas represent highly dense frequency combs. The insets are the zoom-in views of the highly dense frequency combs at wavelengths 3 and 5 μm with the bandwidth of 0.01 nm.

IV. CONCLUSION

In summary, we have designed a multimode As_2Se_3-based strip waveguide and numerically investigate the MIR SC generations when pump pulses launched in the normal dispersion regions of the TE_{00}, TE_{10}, and TE_{20} modes under different wavelengths of pump pulse, peak powers and pulse duration. Highly coherent multi-octave spanning SCs are generated with each of the three modes. When the optimized pump pulse parameters of λ_0=3 μm, P_0=3 kW, and T_0=80 fs are used, the SCs generated with the TE_{00}, TE_{10}, and TE_{20} modes reach 1.82, 1.93, and 2.33 octaves, respectively. All of the SCs generated by the considered three modes are highly coherent even at the noise amplitude η is 0.01. Finally, based on the generated MIR SCs, the octave-spanning frequency comb sources are achieved when a train of 50 pulses at 50 MHz repetition rate is launched into the designed waveguide. It is believed that the generated MIR SC and SC-based frequency comb sources have important applications in

biophotonics, metrology, and sensing. And the exploration of higher-order mode with unique dispersion characteristics to generate the special SCs in one single waveguide for some MIR applications would be of great interest.

REFERENCES

[1] A. Schliesser, N. Picqué, and T. W. Hänsch, "Mid-infrared frequency combs," *Nat. Photon.*, vol. 6, no. 7, pp. 440-449, Jul. 2012.

[2] F. Adler, P. Masłowski, A. Foltynowicz, K. C. Cossel, T. C. Briles, I. Hartl, and J. Ye, "Mid-infrared Fourier transform spectroscopy with a broadband frequency comb," *Opt. Express*, vol. 18, no. 21, pp. 21861-21872, Oct. 2010.

[3] P. Marin-Palomo, J. N. Kemal, M. Karpov, A. Kordts, J. Pfeifle, M. H. P. Pfeiffer, P. Trocha, S. Wolf, V. Brasch, M. H. Anderson, R. Rosenberger, K. Vijayan, W. Freude, T. J. Kippenberg, and K. Koos, "Microresonator-based solitons for massively parallel coherent optical communications," *Nature*, vol. 546, no. 7657, pp. 274-279, Jun. 2017.

[4] V. Torres-Company, J. Schröder, A. Fülöp, M. Mazur, L. Lundberg, Ó. B. Helgason, M. Karlsson, and P. A. Andrekson, "Laser Frequency Combs for Coherent Optical Communications," *J. Lightwave Technol.*, vol. 37, no. 7, pp. 1663-1670, Apr. 2019.

[5] T. Udem, R. Holzwarth, and T. W. Hänsch, "Optical frequency metrology," *Nature*, vol. 416, no. 6877, pp. 233–237, Mar. 2002.

[6] T. J. Kippenberg, R. Holzwarth, and S. A. Diddams, "Microresonator based optical frequency combs," *Science*, vol. 332, no. 6029, pp. 555–559, Apr. 2011.

[7] F. Li, J. H. Yuan, Z. Kang, Q. Li, and P. K. A. Wai, "Modeling frequency comb sources," *Nanophotonics*, vol. 5, no. 2, pp. 292-315, Jun. 2016.

[8] B. Kuyken, T. Ideguchi, S. Holzner, M. Yan, T. W. Hänsch, J.V. Campenhout, P. Verheyen, S. Coen, F. Leo, R. Baets, G. Roelkens, and N. Picqué, "An octavespanning mid-infrared frequencycomb generated in a silicon nanophotonic wire waveguide," *Nat. Commun.*, vol. 6, pp. 6310-1-6, Feb. 2015.

[9] A. L. Gaeta, M. Lipson, and T. J. Kippenberg, "Photonic-chip-based frequency combs," *Nat. Photon.*, vol. 13, no. 3, pp. 158–169, Mar. 2019.

[10] N. Nader, A. Kowligy, J. Chiles, E. J. Stanton, H. Timmers, A. J. Lind, F. C. Cruz, D. M. B. Lesko, K. A. Briggman, S. W. Nam, S. A. Diddams, and R. P. Mirin, "Infrared frequency comb generation and spectroscopy with suspended silicon nanophotonic waveguides," *Optica*, vol. 6, no. 10, pp. 1269-1276, Oct. 2019.

[11] T. Herr, V. Brasch, J. D. Jost, C. Y. Wang, N. M. Kondratiev, M. L. Gorodetsky, and T. J. Kippenberg, "Temporal solitons in optical microresonators," *Nat. Photon.*, vol. 8, no. 2, pp. 145–152, Feb. 2014.

[12] H. Hu, F. D. Ros, M. H. Pu, F. H. Ye, K. Ingerslev, E. P. da Silva, M. Nooruzzaman, Y. Amma, Y. Sasaki, T. Mizuno, Y. Miyamoto, L. Ottaviano, E. Semenova, P. Guan, D. Zibar, M. Galili, K. Yvind, T. Morioka, and L. K. Oxenløwe, "Single-source chip-based frequency comb enabling extreme parallel data transmission," *Nat. Photon.*, vol. 12, no. 8, pp. 469-473, Aug. 2018.

[13] J. M. Dudley, G. Genty, and S. Coen, "Supercontinuum generation in photonic crystal fiber," *Rev. Mod. Phys.*, vol. 78, no. 4, pp. 1135–1184, Oct.-Dec. 2006.

[14] L. Zhang, Q. Lin, Y. Yue, Y. Yan, R.G. Beausoleil, A. Agarwal, L.C. Kimerling, J. Michel, A.E. Willner, "On-chip octave-spanning supercontinuum in nanostructured silicon waveguides using ultralow pulse energy," *IEEE J. Sel. Top. Quantum Electron.*, vol. 18, no. 6, pp. 1799–1806, Nov.-Dec. 2012.

[15] J. M. Dudley and S. Coen, "Coherence properties of supercontinuum spectra generated in photonic crystal and tapered optical fibers," *Opt. Lett.*, vol. 27, no. 13, pp. 1180–1182, Jul. 2002.

[16] C. L. Huang, M. S. Liao, W. J. Bi, X. Li, L. L. Hu, L. Zhang, L. F. Wang, G. S. Qin, T. F. Xue, D. P. Chen, and W. Q. Gao, "Ultraflat, broadband, and highly coherent supercontinuum generation in all-solid microstructured optical fibers with all-normal dispersion," *Photon. Res.*, vol. 6, no. 6, pp. 601-608, Jun. 2018.

[17] M. R. Karim, H. Ahmad, B. M. Rahman, "All-normal-dispersion chalcogenide waveguides for ultraflat supercontinuum generation in the mid-infrared region," *IEEE J. Quantum Electron.*, vol. 53, no. 2, pp. 7100106-1-6, Apr. 2017.

[18] M. Sinobad, A. D. Torre, B. Luther-Davis, P. Ma, S. Madden, S. Debbarma, K. Vu, D. J. Moss, A. Mitchell, J.-M. Hartmann, J.-M. Fedeli, C. Monat, and C. Grillet, "Dispersion trimming for mid-infrared supercontinuum generation in a hybrid chalcogenide/silicon-germanium waveguide," *J. Opt. Soc. Am. B*, vol. 36, no.2, pp. A98-A104, Feb. 2019.

[19] Y. Yuan, P. L. Yang, X. F. Peng, Z. F. Cao, S. J. Ding, N. Zhang, Z. J. Liu, P. Q. Zhang, X. S. Wang, and S. X. Dai, "Ultrabroadband and coherent mid-infrared supercontinuum generation in all-normal dispersion Te-based chalcogenide all-solid microstructured fiber" *J. Opt. Soc. Am. B*, vol. 37, no. 2, pp. 227-232, Feb. 2020.

[20] Y. X. Fang, C. J. Bao, Z. Wang, B. Liu, L. Zhang, X. Han, Y. X. He, H. Huang, Y. X. Ren, Z. Q. Pan, and Y. Yue, "Three-octave supercontinuum generation using SiO_2 cladded Si_3N_4 slot waveguide with all-normal dispersion," *J. Lightwave Technol.*, vol. 38, no. 13, pp. 3431-3438, Jul. 2020.

[21] A. M. Heidt, "Pulse preserving flat-top supercontinuum generation in all-normal dispersion photonic crystal fibers," *J. Opt. Soc. Am. B*, vol. 27, no. 3, pp. 550–559, Mar. 2010.

[22] C. L. Huang, M. S. Liao, W. J. Bi, X. Li, L. F. Wang, T. F. Xue, L. Zhang, D. P. Chen, L. L. Hu, Y. Z. Fang, and W. Q. Gao, "Asterisk-shaped microstructured fiber for an octave coherent supercontinuum in a sub-picosecond region," *Opt. Lett.*, vol. 43, no. 3, pp. 486–489, Feb. 2018.

[23] L. Liu, T. L. Cheng, K. Nagasaka, H. T. Tong, G. S. Qin, T. Suzuki, and Y. Ohishi, "Coherent mid-infrared supercontinuum generation in allsolid chalcogenide microstructured fibers with all-normal dispersion," *Opt. Lett.*, vol. 41, no. 2, pp. 392–395, Jan. 2016.

[24] A. M. Heidt, J. S. Feehan, J. H. V. Price, and T. Feurer, "Limits of coherent supercontinuum generation in normal dispersion fibers," *J. Opt. Soc. Am. B*, vol. 34, no. 4, pp. 764-775, Apr. 2017.

[25] I. Gonzalo, R. Engelsholm, M. Sørensen, and O. Bang, "Polarization noise places severe constraints on coherence of all-normal dispersion femtosecond supercontinuum generation," *Sci. Rep.*, vol. 8, pp. 6579-1-13, Apr. 2018.

[26] N. D. Psaila, R. R. Thomson, H. T. Bookey, S. X. Shen, N. Chiodo, R. Osellame, G. Cerullo, A. Jha, and A. K. Kar, "Supercontinuum generation in an ultrafast laser inscribed chalcogenide glass waveguide," *Opt. Express*, vol. 15, no. 24, pp. 15776–15781, Nov. 2007.

[27] B. J. Eggleton, B. Luther-Davies, and K. Richardson, "Chalcogenide photonics," *Nat. Photon.*, vol. 5, no. 3, pp. 141-148, Mar. 2011.

[28] V. Shiryaev and M. Churbanov, "Trends and prospects for development of chalcogenide fibers for mid-infrared transmission," *J. Non-Cryst. Solids*, vol. 377, pp. 225–230, Oct. 2013.

[29] Y. Yu, X. Gai, P. Ma, K. Vu, Z. Y. Yang, R. P. Wang, D.-Y. Choi, S. Madden, and B. Luther-Davies, "Experimental demonstration of linearly polarized 2–10 μm supercontinuum generation in a chalcogenide rib waveguide," *Opt. Lett.*, vol. 41, no. 5, pp. 958-961, Mar. 2016.

[30] M. R. Karim, B. M. A. Rahman, and G. P. Agrawal, "Mid-infrared supercontinuum generation using dispersion-engineered $Ge_{11.5}As_{24}Se_{64.5}$ chalcogenide channel waveguide," *Opt. Express*, vol. 23, no. 5, pp. 6903-6914, Mar. 2015.

[31] T. S. Saini, A. Kumar, and R. K. Sinha, "Broadband mid-infrared supercontinuum spectra spanning 2-15 μm using As_2Se_3 chalcogenide glass triangular-core graded-index photonic crystal fiber," *J. Lightwave Technol.*, vol. 33, no. 18, pp. 3914-3920, Sep. 2015.

[32] T. S. Saini, A. Kumar, and R. K. Sinha, "Design and analysis of dispersion engineered rib waveguides for on-chip mid-infrared supercontinuum," *J. Lightwave Technol.*, vol. 36, no. 10, pp. 1993-1999, May 2018.

[33] X. Yang, Z. H. Xu, S. P. Chen, and Z. F. Jiang, "High power LP_{11} mode supercontinuum generation from an all-fiber MOPA," *Opt. Express*, vol. 26, no. 11, pp. 13740-13745, May 2018.

[34] D. Jain, C. Markos, T. M. Benson, A. B. Seddon, and O. Bang "Exploiting dispersion of higher-order-modes using M-type fiber for application in mid-infrared supercontinuum generation", *Sci. Rep.*, vol. 9, pp. 8536-1-11 Jun. 2019.

[35] Y. Yu, X. Gai, T. Wang, P. Ma, R. P. Wang, Z. Y. Yang, Duk-Yong Choi, S. Madden, and B. Luther-Davies, "Mid-infrared supercontinuum generation in chalcogenides," *Opt. Mater. Express*, vol. 3, no. 8, pp. 1075-1086, Aug. 2013.

[36] M. Veinguer, A. Feigel, B. Sfez, M. Klebanov, V. Lyubin, "New application of inorganic chalcogenide photoresists in lift-off photolitography," *J. Optoelectron. Adv. Mater.*, vol. 5, no. 5, pp. 1361-1364, Aug. 2003.
[37] J. J. Hu, V. Tarasov, N. Carlie, N.-N. Feng, L. Petit, A. Agarwal, K. Richardson, and L. Kimerling, "Si-CMOS-compatible lift-off fabrication of low-loss planar chalcogenide waveguides," *Opt. Express*, vol. 15, no. 9, pp. 11798-11807, Sep. 2007
[38] K. Suzuki, K. Ogusu, and M. Minakata, "Single-mode Ag-As2Se3 strip-loaded waveguides for applications to all-optical devices," *Opt. Express*, vol. 13, no. 21, pp. 8634-8641, Oct. 2005
[39] Y. L. Ruan, W. T. Li, R. Jarvis, N. Madsen, A. i Rode, and B. Luther-Davies, "Fabrication and characterization of low loss rib chalcogenide waveguides made by dry etching," *Opt. Express*, vol. 12, no. 21, pp. 5140-5145, Oct. 2004.
[40] Z. D. Fan, K. L. Yan, L. M. Zhang, J. S. Qin, J. B. Chen, R. P. Wang, and X. Shen, "Design and fabrication of As_2Se_3 chalcogenide waveguides with low optical losses," *Appl. Opt.*, vol. 59, no. 6, pp. 1564-1568, 2020.
[41] Y. Yu, X. Gai, P. Ma, K. Vu, Z. Y. Yang, R. P. Wang, D.-Y. Choi, S. Madden, and B. Luther-Davies, "Experimental demonstration of linearly polarized 2–10 μm supercontinuum generation in a chalcogenide rib waveguide," *Opt. Let.*, vol. 41, no. 5, pp. 958-961, Mar. 2016.
[42] B. Ung and M. Skorobogatiy, "Chalcogenide microporous fibers for linear and nonlinear applications in the mid-infrared," *Opt. Express*, vol. 18, no. 8, pp. 8647–8659, Apr. 2010.
[43] G. P. Agrawal, *Nonlinear Fiber Optics*, 5th ed. Oxford, UK: Academic, 2013, pp. 8-39.
[44] B. Ung and M. Skorobogatiy, "Chalcogenide microporous fibers for linear and nonlinear applications in the mid-infrared," *Opt. Express*, vol. 18, no. 8, pp. 8647-8659, Apr. 2010.
[45] H. Lin, Z. Yi, S. Danto, J. D. Musgraves, and J. Hu, "Mid-infrared As_2Se_3 chalcogenide glass-on-silicon waveguides," in *Proceedings of IEEE Conference on The 9th International Conference on Group IV Photonics (GFP) (IEEE 2012)*, pp. 246–248.
[46] F. Li, Q. Li, J. H. Yuan, and P. K. A. Wai, "Highly coherent supercontinuum generation with picosecond pulses by using self-similar compression," *Opt. Express*, vol. 22, no. 22, pp. 27339-27354, Oct. 2014.
[47] Y. J. Cheng, J. H. Yuan, C. Mei, F. Li, Z. Kang, B. B. Yan, X. Zhou, Q. Wu, K. R. Wang, X. Z. Sang, K. P. Zhong, C. X. Yu, and G. Farrell, "Self-similar picosecond pulse compression for supercontinuum generation at mid-infrared wavelength in silicon strip waveguides," *Opt. Commun.*, vol. 454, pp. 124380-1-7, Jan. 2020.
[48] J. Hult, "A fourth-order Runge-Kutta in the interaction picture method for simulating supercontinuum generation in optical fibers," *J. Lightwave Technol.*, vol. 25, no. 12, pp. 3770–3775, Dec. 2007.
[49] T. Zhu, Y. Hu, P. Gatkine, S. Veilleux, J. Bland-Hawthorn and M. Dagenais, "Ultrabroadband High Coupling Efficiency Fiber-to-Waveguide Coupler Using Si_3N_4/SiO_2 Waveguides on Silicon," *IEEE Photonics Journal*, vol. 8, no. 5, pp. 1-12, Oct. 2016.
[50] Y. H. Ding, J. Xu, F. D. Ros, B. Huang, H. Y. Ou, and C. Peucheret, "On-chip two-mode division multiplexing using tapered directional coupler-based mode multiplexer and demultiplexer," *Opt. Express*, vol. 21, no. 8, pp. 10376-10382, Apr. 2013.
[51] Z. L. Zhang, X. Hu and J. Wang, "On-chip optical mode exchange using tapered directional coupler," *Sci. Rep.*, vol. 5, pp. 16072-1-7, Nov. 2015.
[52] E. A. Anashkina, A. V. Andrianov, M. Yu. Koptev, S. V. Muravyev, and A. V. Kim, "Generating femtosecond optical pulses tunable from 2 to 3 μm with a silica-based all-fiber laser system," *Opt. Lett.*, vol. 39, no. 10, pp. 2963–2966, May 2014.
[53] G. Soboń, T. Martynkien, P. Mergo, L. Rutkowski, and A. Foltynowicz, "High-power frequency comb source tunable from 2.7 to 4.2 μm based on difference frequency generation pumped by an Yb-doped fiber laser," *Opt. Lett.*, vol. 42, no. 9, pp. 1748–1751, May 2017.
[54] J. Chiles, N. Nader, E. J. Stanton, D. Herman, G. Moody, J. Zhu, J. C. Skehan, B. Guha, A. Kowligy, J. T. Gopinath, K. Srinivasan, S. A. Diddams, I. Coddington, N. R. Newbury, J. M. Shainline, S. W. Nam, and R. P. Mirin, "Multifunctional integrated photonics in the mid-infrared with suspended AlGaAs on silicon," *Optica*, vol. 6, no. 9, pp. 1246–1254, Sep. 2019.

YUJUN CHNEG was born in China. He received the B.S. degree from Zhengzhou University, Zhengzhou, China, in 2016. He is currently pursuing the Ph.D. degree at Beijing University of Posts and Telecommunications, Beijing, China. His research interests include on-chip supercontinuum generation, frequency comb generation, pulse compression, and other nonlinear dynamics in optical devices and optical systems.

JINHUI YUAN (Senior Member, IEEE) received the B.S. and M.S. degrees from Yan Shan University, Qinhuangdao, China, in 2005 and 2008, respectively. In 2011, he received the Ph.D. degree from Beijing University of Posts and Telecommunications (BUPT), Beijing, China. Now he is with the BUPT as an associate professor. .He was select as a Hong Kong Scholar with the Photonics Research Centre, Department of Electronic and Information Engineering, The Hong Kong Polytechnic University, in 2013. He has published more than 200 articles in the academic journals and conferences. His current research interests include photonic crystal fibers, silicon waveguide, and optical fiber devices. He is also a member of OSA. His current research interests include photonic crystal fibers, silicon waveguide, and optical fiber devices. He is the Senior Members of OSA.

CHAO MEI received the B.S. degree of Optical Information Science Technology from Harbin Engineering University, Harbin, China in 2013. He has received the Ph.D. degree of Optical Engineering in Beijing University of Posts and Telecommunication, Beijing, China in 2019. Now he is a postdoc at Max-Born institute for nonlinear optics and short pulse spectroscopy, Berlin, Germany and cooperates with University of Science and Technology Beijing, Beijing, China. He is a member of IEEE. His research interests are ultrafast optics, nonlinear optics, pulse shaping, nano optics, and nonlinear dynamics in optical devices and optical systems.

FENG LI received the B.S. and Ph.D. degrees from University of Science and Technology of China, Hefei, China, in 2001 and 2006, respectively. After that, he joined the Hong Kong Polytechnic University as a Postdoctoral Fellow. Currently he is a Research Assistant Professor at the Hong Kong Polytechnic University. His research interests include fiber lasers, especially multiwavelength lasers and mode locked lasers, nonlinear fiber optics, supercontinuum generation, and nonlinear dynamics in optical devices and optical systems.

XIAN ZHOU received the Ph.D. degree in electromagnetic field and microwave technology from Beijing University of Posts and Telecommunications (BUPT), Beijing, China, in 2011. She is currently a Professor at the Department of computer and communication engineering, University of Science and Technology Beijing (USTB). She was selected as a Hong Kong Scholar at the Photonics Research Centre, Department of Electronic and Information Engineering, The Hong Kong Polytechnic University, in 2013. Her research interests are focused on high-speed optical communications, short reach communications, and digital signal processing. She has published over 150 papers in the academic journals and conferences.

QIANG WU received the B.S. and Ph.D. degrees from Beijing Normal University and Beijing University of Posts and Telecommunications, Beijing, China, in 1996 and 2004, respectively. From 2004 to 2006, he worked as a Senior Research Associate in City University of Hong Kong. From 2006 to 2008, he took up a research associate post in Heriot-Watt University, Edinburgh, U.K. From 2008 to 2014, he worked as a Stokes Lecturer at Photonics Research Centre, Dublin Institute of Technology, Ireland. He is an Associate Professor / Reader with Faculty of Engineering and Environment, Northumbria University, Newcastle Upon Tyne, United Kingdom. His research interests include optical fiber interferometers for novel fiber optical couplers and sensors, nanofiber, microsphere sensors for bio-chemical sensing, the design and fabrication of fiber Bragg grating devices and their applications for sensing, nonlinear fibre optics, surface plasmon resonant and surface acoustic wave sensors. He has over 200 publications in the area of photonics and holds 3 invention patents. He is an Editorial Board Member of Scientific Reports, an Associate Editor for IEEE Sensors Journal and an Academic Editor for Journal of Sensors.

BINBIN YAN received the B.S. and M.S. degrees from Beijing University of Posts and Telecommunications (BUPT), Beijing, China, in 2003 and 2005, respectively. In 2009, she received the Ph.D. degree from BUPT. Now she is with the BUPT as an Associate Professor. Her research interests include photonic devices and fiber optic sensing.

KUIRU WANG received the B.S. and M.S. degrees from Beijing University of Posts and Telecommunications (BUPT), Beijing, China, in 1984 and 1990, respectively. In 2009, she received the Ph.D. degree from BUPT. Now she is with the BUPT as a Professor. Her current research interests include optical fiber communication and photonic devices.

CHONGXIU YU graduated from the Beijing University of Posts and Telecommunications (BUPT), Beijing, China, in 1969. Now she is with the BUPT as a Professor. She is engaged in university education and research work and has been the Principal Investigator of many projects supported by China 863 plan, the National Natural Science Foundation and the National Ministry of Science Technology, and so on. Up to now she has published more than 300 papers. Her Research interests are the optical fiber communication, photonic switching, and optoelectronics technology and its applications. Prof. Yu is the Members of Chinese Institute of Communication, Committee of Fiber Optics and Integral Optics, and Chinese Optical Society.

KEPING LONG (Senior Member, IEEE) received the M.S. and Ph.D. degrees from the University of Electronic Science and Technology of China, Chengdu, China, in 1995 and 1998, respectively. From September 1998 to August 2000, he was a Postdoctoral Research Fellow with the National Laboratory of Switching Technology and Telecommunication Networks, Beijing University of Posts and Telecommunications (BUPT), Beijing, China. From September 2000 to June 2001, he was an Associate Professor with BUPT. From July 2001 to November 2002, he was a Research Fellow with the ARC Special Research Centre for Ultra Broadband Information Networks, University of Melbourne, Melbourne, Australia. He is currently a Professor and Dean with the School of Computer and Communication Engineering, University of Science and Technology Beijing. He has authored more than 200 papers and has delivered 20 keynote speeches. He is a Member of the Editorial Committee of Sciences in China Series F and China Communications. His research interests are optical internet technology, new-generation network technology, wireless information networks, value-added service, and secure technology of networks. Dr. Long has been a Technical Program Committee (TPC) and International Steering Committee member for COIN2003/04/05/06/07/08/09/10, IEEE IWCN2010, ICON04/06, and APOC2004/06/08; a Co-chair of the organization membership for the 2006 International Wireless Communications and Mobile Computing Conference; the TPC chair of COIN2005/2008; and a TPC Cochair of COIN2008/2010. He has been invited to talk at both international and local conferences. He received the National Science Fund for Distinguished Young Scholars of China in 2007 and was selected as the Chang Jiang Scholars Program Professor of China in 2008.

P.K.A. WAI (Fellow, IEEE) received the B.S. (Hons.) degree from the University of Hong Kong, Hong Kong, in 1981, and the M.S. and Ph.D. degrees from the University of Maryland, College Park, MD, USA, in 1985 and 1988, respectively. In 1988, he joined Science Applications International Corporation, McLean, VA. In 1990, he became a Research Associate with the University of Maryland. In 1996, he joined the Department of Electronic and Information Engineering, The Hong Kong Polytechnic University. In 2005, he became a Chair Professor of Optical Communications. He is an active contributor to the field of photonics and optical communications, having authored or coauthored more than 300 international refereed publications. His research interests include soliton, fiber lasers, modeling and simulations of optical devices, long-haul optical fiber communications, all-optical packet switching, and network theories. Prof. P.K.A. Wai is the Fellow of the OSA.